Numerical Study of a DFB Semiconductor Laser and Laser Array With Chirped Structure Based on the Equivalent Chirp Technology

Yitang Dai and Jianping Yao, *Senior Member, IEEE*

Abstract—We propose that a Bragg grating with a chirp profile in a semiconductor distributed feedback (DFB) laser can be designed and fabricated through nonuniform sampling of a uniform grating based on the equivalent chirp technology (ECT). The characteristics, including the relationship between the input current and output power, the light distribution within the laser cavity, the lasing spectrum, and the linewidth, are numerically analyzed and compared with a DFB laser with a true chirped grating. The study shows that the proposed DFB laser with an equivalent chirp provides an identical performance to that of a conventional DFB laser. Based on the ECT, different chirp gratings in a DFB laser array can also be fabricated by simply using different sampling functions, with the grating period in all gratings kept constant. The key advantage of the proposed technique is that a DFB laser or laser array can be fabricated based on the conventional holography technology, which would simplify the fabrication.

Index Terms—Bragg grating, distributed feedback (DFB) laser, nonuniformly spaced sampling.

I. INTRODUCTION

ADVANCED semiconductor lasers are key devices in high-bit-rate long-haul optical fiber communication systems. Among many different laser structures, the distributed feedback (DFB) structure has been widely employed in semiconductor lasers to achieve single-longitudinal-mode operation with a precise spectral control. Although the grating in a DFB laser can be fabricated based on simple holography technology, the grating with uniform period is not suitable for single-longitudinal-mode operation because of the mode degeneracy. The introduction of a quarter-wave phase shift to the grating period would generate an ultranarrow transmission band, which would ensure a single-longitudinal-mode operation [1]. To improve the lasing performance, a grating with a sophisticated chirp profile is also needed, which would ensure a single-longitudinal-mode operation and at the same time suppress unwanted spatial hole burning (SHB) resulted from the quarter-wave phase shift. For example, the corrugation-pitch modulation (CPM), where a quarter-wave phase shift is distributed at a phase-arranging

region (PAR) rather than a single quarter-wave jump at the center of the grating, has been proven to be capable of suppressing the SHB effect, providing a more uniform longitudinal field distribution and increasing the single-longitudinal-mode operation stability [2], [3]. Other performances can also be improved if an appropriately designed chirped grating is used [4], [5]. The grating chirp has also found other applications in advanced DFB semiconductor lasers. For example, in [6], an optimized continuous chirp was used to correct the unwanted effective refractive index along a tapered waveguide. Since a true chirp requires a precise control of each grating line, advanced fabrication technology such as a carefully designed e-beam should be used [7]. Other techniques for a DFB structure with a chirp profile include varying the stripe width [8] or bending the waveguides [9], [10], which may show difficulty in the waveguide fabrication since a precise control of the waveguide shape is required.

In addition to individual DFB lasers, DFB laser arrays and wavelength-selectable laser sources are also highly desirable especially in dense wavelength-division multiplexing (DWDM) systems [11], [12]. Such a light source contains multiple DFB lasers with different lasing wavelengths on a single chip, and conventionally each laser is manufactured with a slightly different grating pitch. This usually requires the definition of multiple grating sections with different pitch lengths. Using e-beam lithography would cause obvious high costs. Even by holography, numerous exposures for different gratings with different periods have to be performed side by side on the wafer, which requires multiple alignment changes. In [13], a technology based on a homogeneous grating (constant pitch length) on the whole wafer was demonstrated to realize a DFB laser array, which is really at low cost. However, in the design, the waveguides should be bent, with the grating in each laser being tilted, which may couple the light out of the laser cavity.

Our recently developed equivalent chirp technology (ECT) shows a high potential to realize a complicated chirp in a DFB laser and a DFB laser array without using e-beam lithography. The ECT, based on nonuniform sampling in a sampled Bragg grating (SBG) with uniform grating period, has been demonstrated to be able to achieve complicated frequency responses in a fiber Bragg grating (FBG) [14]–[16]. The same concept has also been recently applied to the design of a semiconductor DFB laser to introduce discrete phase shifts in the laser cavity [17]. Such an ECT-based DFB laser has the advantage that the imbedded grating is simply an SBG with homogeneous grating period that can be fabricated with the conventional holography

technology. In this paper, the theory of the ECT-based DFB laser is developed. We show that a continuous phase modulation, such as the CPM, can be realized based on the ECT. We also show that an ECT-based SBG is equivalent to a regular chirped Bragg grating in a DFB laser. In addition, we demonstrate that a DFB laser array can also be designed based on the ECT, which can be fabricated based on a homogeneous grating in the entire wafer, without the requirement for bending the waveguides or tilting the grating.

The remainder of this paper is organized as follows. In Section II, a theoretical discussion of the ECT is presented. The equivalence between an ECT-based DFB laser with an equivalent chirp and a DFB laser with a true chirp is demonstrated theoretically. A CPM DFB laser is then designed based on the ECT. In Section III, a detailed numerical study on the proposed DFB laser is presented. The characteristics, including the relationship between the input current and output power, the light distribution within the laser cavity, the lasing spectrum, and the linewidth, are compared with a DFB laser with a true chirp. In Section IV, the impact of the sampling period and the duty cycle of an SBG on the performance of the proposed DFB laser are studied. The implementation of a DFB laser array based on the ECT is also discussed in this section. A conclusion is drawn in Section V.

II. PRINCIPLE

Conventionally, an SBG is implemented based on uniform sampling which is often used in a laser cavity to realize multiwavelength operation, since an SBG has multiple reflection channels. In an ECT-based SBG, however, only a single channel would be used (the $\pm$1st channel is usually selected thanks to the large reflectivity). In this paper, the $-$1st channel is considered. Although the grating period is uniform, the SBG could have exactly the same characteristics as a regular chirped grating in the channel of interest. The required chirp is generated equivalently by the nonuniform sampling.

Mathematically, the index modulation change $\Delta n(z)$ of an ECT-based SBG can be described by

$$\Delta n(z) = \frac{1}{2} s(z) \exp\left(j \frac{2\pi z}{\Lambda}\right) + c.c \qquad (1)$$

where Λ is the grating period and $s(z)$ is the nonuniform sampling function given by

$$s(z) = s_0 \left[z - \frac{\varphi(z)}{2\pi} P\right] \qquad (2)$$

where $s_0(z)$ is a periodic sampling function, which is usually a square wave, with a period of P and a duty cycle of γ, and $\varphi(z)$ is the chirp function which can be achieved equivalently by the nonuniform sampling. Based on the Fourier series expansion, we have

$$s_0(z) = \sum_m F_m \exp\left(j \frac{2\pi m}{P} z\right) \qquad (3)$$

where F_m is the mth-order Fourier coefficient. Substituting (2) and (3) into (1), we have

$$\Delta n(z) = \sum_m \frac{1}{2} F_m \exp\left[-jm\varphi(z) + j\frac{2\pi z}{\Lambda_m}\right] + c.c \qquad (4)$$

where

$$\Lambda_m = \frac{\Lambda P}{m\Lambda + P} \approx \Lambda - m\frac{\Lambda^2}{P}. \qquad (5)$$

As can be seen from (4), the SBG is actually a superposition of many subgratings with different grating periods, Λ_m, with each subgrating having a spectral response corresponding to one of the multiple channels. Based on (5), the channel spacing is determined by P. When P is sufficiently small, the spectral response of the $-$1st subgrating is not overlapped with the spectral responses of the adjacent sub-gratings. Therefore, the SBG is equivalent to a regular chirped grating in the $-$1st channel. In the design, we can choose a proper P such that the $-$1st channel is located within the gain spectrum of the semiconductor material (a width of about 30 nm), while all of the other channels are located outside the gain spectrum. Therefore, only the wavelength within the $-$1st channel is possible to lase. Based on the analysis, we conclude that, in the proposed DFB laser, the SBG is equivalent to a regular SFB in the $-$1st subgrating, which has a grating function given by

$$\Delta n_{-1}(z) = \frac{1}{2} F_{-1} \exp\left[j\varphi(z) + j\frac{2\pi z}{\Lambda_{-1}}\right] + c.c. \qquad (6)$$

Then, the desired chirp modulation $\varphi(z)$ is realized equivalently in a phase-modulation-free SBG using the ECT.

In the following, we will design a DFB laser with a chirped grating in the cavity based on the ECT. To have a narrow transmission band in the imbedded grating to ensure a single-longitudinal-mode operation, a phase modulation should be introduced. It could be a single π-phase shift at the center of the grating or a π-phase shift that is distributed at a phase-arranging region (PAR), which is called CPM. In this paper, we assume that the phase changes linearly within the PAR given by

$$\varphi(z) = \begin{cases} 0, & -L/2 \leq z < -D/2 \\ \frac{\pi}{D} \times \left(z + \frac{D}{2}\right), & -D/2 \leq z < D/2 \\ \pi, & D/2 \leq z < L/2 \end{cases} \qquad (7)$$

where L and D are, respectively, the lengths of the grating and the PAR. The phase distribution function $\varphi(z)$ is illustrated in Fig. 1(a). Based on the required phase modulation, the grating in a CPM DFB laser is then illustrated in Fig. 1(c). For comparison, a grating with a uniform period is shown Fig. 1(b).

Based on (2), we get the sampling function of the grating in the ECT-based CPM DFB laser. Since $\varphi(z)$ is now nonlinear within the whole grating length, $s(z)$ is then a nonuniform sampling function because the sampling period P_s changes nonlinearly with the position, which is given by

$$P_s(z) = \begin{cases} P, & \text{out of PAR} \\ \frac{P}{1-P/2D}, & \text{within PAR}. \end{cases} \qquad (8)$$
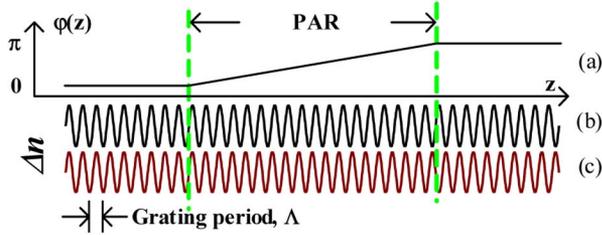
Fig. 1. (a) Phase distribution of a grating in a CPM DFB laser. The π-phase shift is distributed linearly in the PAR. (b) Index modulation of a grating with a uniform period of Λ. (c) Grating in the CPM DFB laser. It can be seen that the grating has a π-phase difference at the right side compared with the uniform grating.
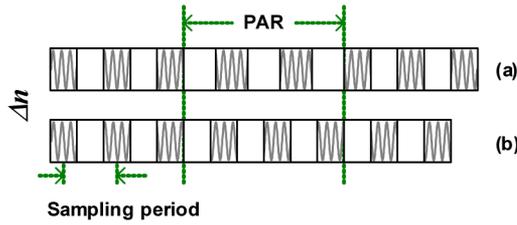
Fig. 2. (a) Nonperiodic sampling function $s(z)$ used to realize the equivalent chirp in a CPM DFB laser. The grating period is a constant along the grating. (b) Conventional sampling function $s_0(z)$ with a period of P.

The nonuniform sampling is illustrated in Fig. 2(a). In our design, $s_0(z)$ is a square wave with a duty cycle of $\gamma = 0.5$, which is shown in Fig. 2(b) as a comparison with the nonuniform sampling function.

To demonstrate that the proposed SBG has the same spectral characteristics as a regular CPM grating, we calculate the transmission spectral responses for both gratings based on the well-known transmission matrix method. As we will discuss in Section III, for an SBG with a small sampling period P, the lasing would start at the -1st channel, so here our analysis will be focused on the -1st channel. In the ECT-based CPM DFB laser, the lengths of the entire grating and the PAR are, respectively, $L = 400 \ \mu$m and $D = 200 \ \mu$m. The sampling period P is 6.25 μm, which gives a total number of samples of 64. The transmission spectrum of the SBG is calculated and plotted as the solid line in Fig. 3. The parameters used in the simulations are listed in Table I. As a comparison, a chirped grating for a regular CPM DFB laser that has the same grating and PAR lengths is also simulated, with the transmission spectrum plotted as the dotted line in Fig. 3. As can be seen, the SBG has the same transmission spectrum within the band of interest as that of the regular CPM grating, with a gap mode to form the desired resonance cavity. The results show that the chirp-free SBG in (1) is equivalent to the grating with a true chirp in (6), thanks to the equivalent chirp introduced by the nonuniform sampling.

It should be noted that the gap mode in the CPM DFB laser is not at the center of the stop band, as can be seen from Fig. 3. Although a gap mode at the center will lead to the best side-mode suppression ratio (SMSR), the distributed phase shift can significantly reduce the light concentration in the cavity of a quarter-wave phase shift laser and then reduce the SHB. Therefore, there is a tradeoff between the SMSR and reduction of light concentration. The optimization of the length of the PAR will depend
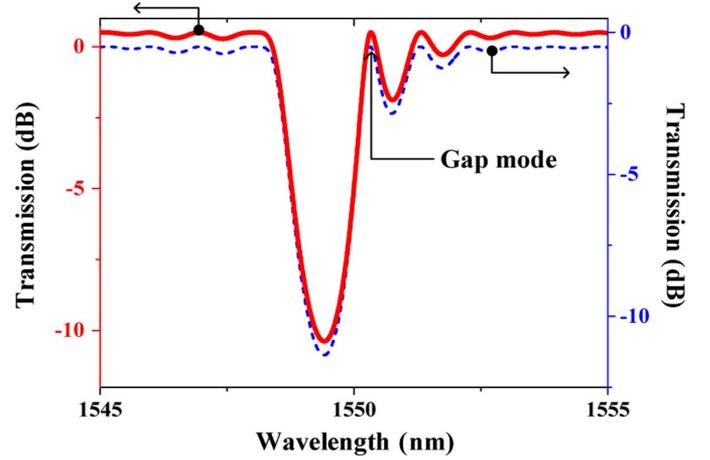
Fig. 3. Transmission spectra of the regular chirp grating (dotted line) and the SBG with an equivalent chirp at the -1st channel (solid line) around 1550 nm. Identical spectral characteristics are observed.

TABLE I
PARAMETERS USED IN OUR SIMULATION

Cavity length (L)	400 μm
Length of the PAR (D)	200 μm
Effective refractive index (n_{eff})	3.43
Period of the regular chirped grating (Λ_C)	225.948 nm
Index modulation of the regular chirped grating (κ_C)	50 cm^{-1}
Grating period of the equivalent CPM grating (Λ)	218.062 nm
Index modulation of the equivalent CPM grating (κ)	150 cm^{-1}
Sampling period of the equivalent CPM grating (P)	6.25 μm
Duty cycle of the equivalent CPM grating (γ)	0.5
Slope of gain–carrier density relationship (α)	3×10^{-16} cm^2
Transparency carrier density (N_t)	1.5×10^{18} cm^{-3}
Coupling of mode to active layer (Γ)	0.35
Linewidth enhancement factor (β_C)	1.5
Linear carrier lifetime (τ)	4ns
Waveguide absorption and scattering loss (α_L)	5 cm^{-1}
Active layer thickness (d)	0.18 μm
Current stripe width (W)	3.5 μm
Bimolecular carrier recombination coefficient (B)	1×10^{-10} cm^{3}s^{-1}
Effective optical width perpendicular to junction (d_{eff})	0.47 μm
Far-field pattern FWHM perpendicular to junction (θ_d)	50°
Effective optical width parallel to junction (W_{eff})	3.5 μm
Far-field pattern FWHM parallel to junction (θ_W)	20°
Width of spontaneous emission (Δf_{sp})	80 nm

on the above tradeoff [18]. In addition, since the DFB laser based on ECT acts the same as a conventional DFB laser does, the facet reflection will also decrease the lasing performance. Therefore, an anti-reflection (AR) coating is also required in an ECT-based DFB laser.

III. SINGLE-WAVELENGTH EQUIVALENT CPM DFB LASER

Here, the lasing performance of the equivalent CPM DFB laser is numerically studied based on the spectral domain model developed in [19]–[22]. Using this model, the static characteristics of the proposed DFB laser with an equivalent chirp is evaluated. As a comparison, a regular CPM DFB laser is also analyzed. The parameters used in the numerical simulations are also listed in Table I.

Fig. 4 shows the power–injection current (P-I) performance of the two DFB lasers at the 1550-nm band. As can be seen, the two lasers have identical performances. In our design, the
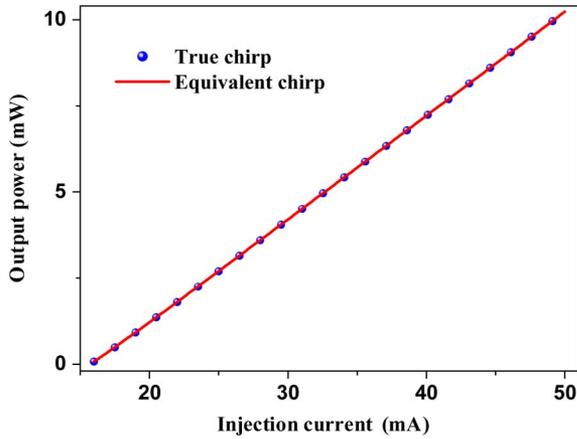
Fig. 4. P–I curve of the DFB semiconductor laser with true (dotted line) and equivalent (solid line) CPM.
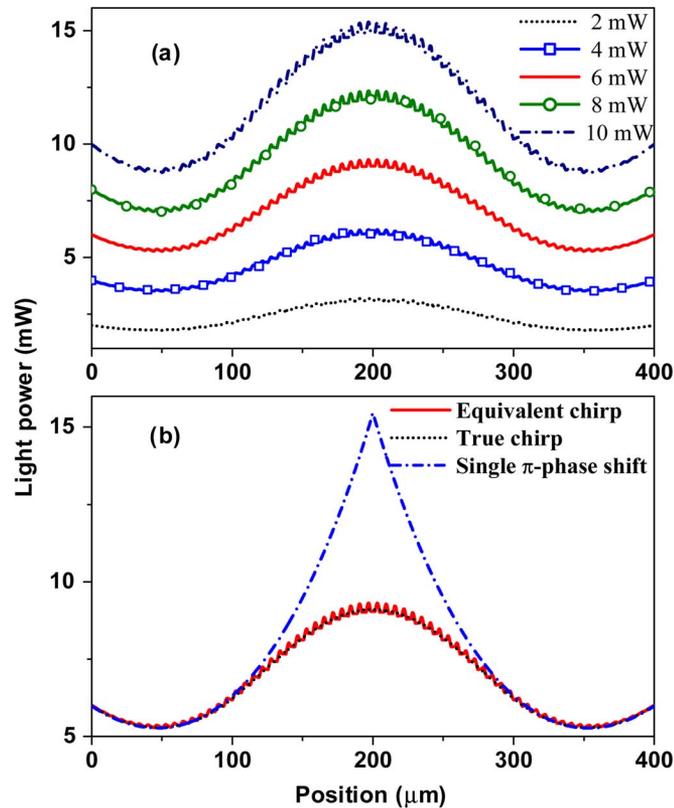
Fig. 5. (a) Optical intensity distributions for the equivalent CPM DFB laser when the output power levels are 2, 4, 6, 8, and 10 mW. (b) Optical intensity distributions of the DFB lasers with an equivalent chirp, a true chirp, and a single π-phase shift when the output power is 6 mW.

Fig. 6. (a) Spectra of the equivalent CPM DFB laser when the output power levels are 2, 4, 6, 8, and 10 mW. (b) Spectra of the DFB lasers with an equivalent chirp and a true chirp when the output power is 6 mW.

wavelength difference between the lasing channel and its adjacent channels is as large as 50 nm. As a result, the gain at the adjacent channels is much lower than that in the lasing channel in the 1550-nm band. We have demonstrated that such a design provides a sufficiently large threshold margin in the equivalent DFB laser [17], which ensures a single-longitudinal-mode operation with a high output power.

Fig. 5(a) shows the light-intensity distributions along the cavity at different output power levels for the ECT-based DFB laser. When the injection current is 36 mA, which corresponds

to an output power of about 6 mW for both DFB lasers, the light-intensity distributions are calculated and plotted in Fig. 5(b). The two lasers have almost the same in-cavity light distributions. The intensity distribution ripples in the equivalent DFB laser are resulted from the sampled structure of the grating. As a comparison, the light distribution in a DFB laser with a single π-phase shift is also calculated and plotted in Fig. 5(b). In the simulation, the parameters for this single π-phase shift DFB laser are the same as those in Table I, except that the length of the PAR, D, is zero. The output power is also 6 mW at the input current of 36 mA. Compared with the π-phase-shift DFB laser, the light in the CPM DFB laser is distributed in the PAR, rather than a sharp and much higher peak at the π-phase-shift point. With a more uniform lasing light distribution, the CPM DFB laser has been demonstrated to provide a more stable single-longitudinal-mode operation, even at a high output power [2]–[5].

The spectrum of the proposed DFB laser is calculated based on the spectral model in [21], where the spontaneous emission is considered when the device is lasing. Fig. 6(a) shows the lasing spectra under different output power levels. When the output power is 6 mW, the spectra of the DFB lasers with an equivalent and a true chirp are plotted in Fig. 6(b). One can see that the two DFB lasers have the same SMSR that is greater than 70
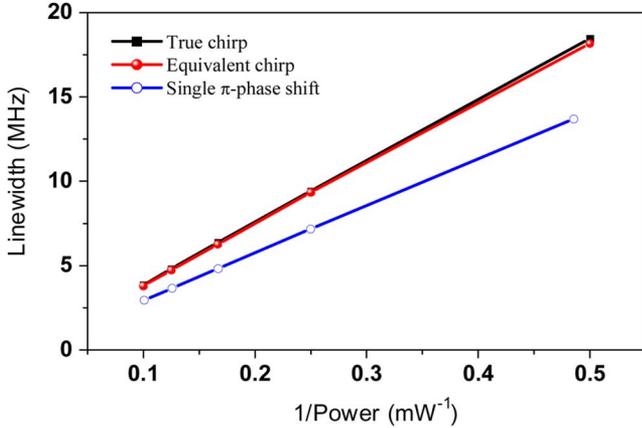
Fig. 7. Linewidth/output power relationship of the DFB lasers with an equivalent chirp and a true chirp. The relationship between the linewidth and the output power of the DFB laser with a single π-phase shift is plotted for comparison.

dB. Another important performance measure is the linewidth of the lasing output, which is also evaluated based on the model in [21], where the spontaneous emission is considered. Fig. 7 shows the relationship between the linewidth and the output power of the DFB lasers with an equivalent chirp and a true chirp. The result clearly shows that the two DFB lasers provide an identical performance. Compared with a conventional DFB laser with a single π-phase shift, the line width of the CPM laser is a little wider, which comes from the asymmetry of the gap mode, as can be seen from Fig. 3, where the gap mode is not at the center of the stop band, and it is a cost paid for getting a more uniform light distribution in the laser cavity.

From the above analysis, we can conclude that a DFB laser with an equivalent CPM provides the same performance as a DFB laser with a true CPM. The advantage of the equivalent DFB laser is that the laser has a uniform grating structure, which can be fabricated by the conventional holography technology without the need for precise line-by-line control.

IV. EQUIVALENT CPM DFB LASER ARRAY

In the proposed DFB laser, the imbedded grating has a sampled structure. Two important parameters are associated with the design of the SBG: the sampling period P and the duty cycle γ. Here, the two parameters on the lasing performance are analyzed.

A. Duty Cycle

From (6), we can see that the index modulation depth of the -1st subgrating is F_{-1}, which is the coefficient of the -1st Fourier component of the sampling function $s_0(z)$. For practical implementation, the sampling function can be approximated by a square wave. Then, F_{-1} will change as a function of the duty cycle of the sampling function

$$|F_{-1}| = \left| \frac{\sin(\pi\gamma)}{\pi} \right| \times \Delta n_s \quad (9)$$

where Δn_s is the index modulation depth of the SBG. The relationship between F_{-1} and γ is plotted in Fig. 8.
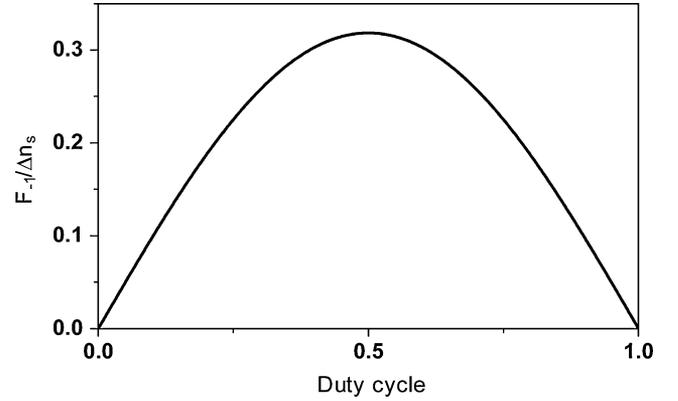
Fig. 8. Relationship between F_{-1} and the duty cycle of the SBG.
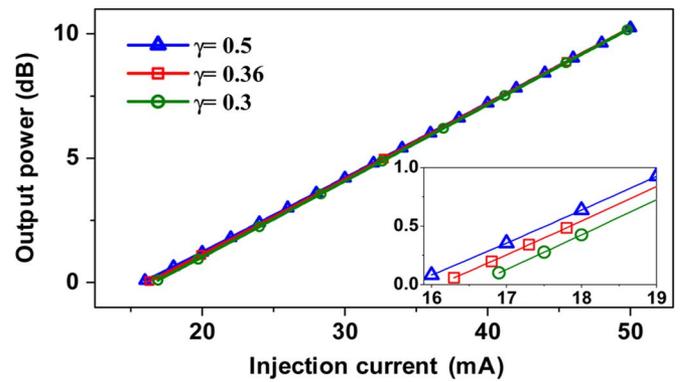
Fig. 9. P–I curve of the equivalent DFB laser with duty cycles of 0.3, 0.36, and 0.5. The insert shows the threshold variation induced by the duty cycle change.

F_{-1} is the index modulation depth of the -1st subgrating, which can be considered as the effective index modulation depth in the laser cavity. On one hand, F_{-1} is less than the actual index modulation depth of the SBG Δn_s, as shown in Fig. 8. To maximize the effective index modulation depth, a duty cycle of $\gamma = 0.5$ should be selected. Therefore, the index modulation used in the ECT should be approximately three times higher than that in a conventional DFB laser. In the fabrication of an ECT-based DFB laser, a stronger or longer grating is required. On the other hand, by controlling the duty cycle of the SBG, we can control the effective index modulation depth to the desired value, instead of controlling the actual index modulation of the SBG. Fig. 9 shows the lasing performance of the equivalent CPM DFB laser with different duty cycles. As shown in Fig. 8, when the duty cycle decreases from 0.5, the effective coupling coefficient will also decrease, and then the ability of the DFB cavity to confine the light will decrease. Therefore, the threshold will increase, as shown in the insert of Fig. 9. Similarly, the linewidth and the SMSR at a given output optical power will increase and decrease, respectively, as shown in Fig. 10. It can be seen that the induced performance change by the duty cycle is the same as that when the coupling coefficient of a conventional DFB laser is changed, which confirms that the control of the duty cycle is equivalent to the control of the coupling coefficient of a DFB laser.

In addition, when the duty cycle is 0.5, which is a conventionally used value, the performance change induced by the duty
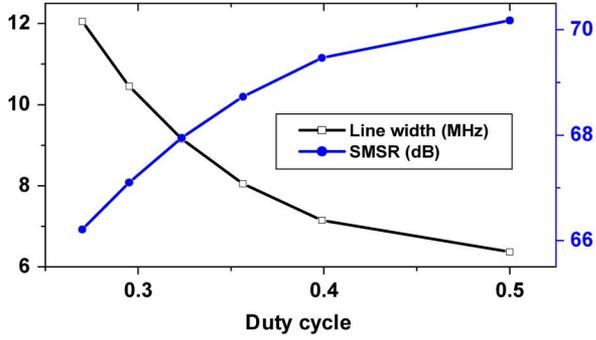
Fig. 10. Linewidth and the SMSR change versus the change of the sampling duty cycle. The output optical power is 6 dBm.
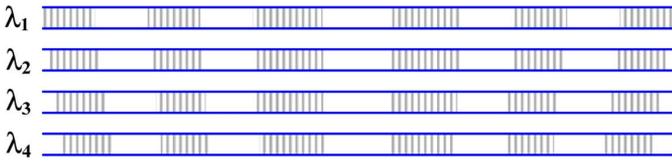
Fig. 11. Illustration of a CPM DFB laser array implemented based on the ECT. Different lasing wavelengths and chirps are obtained by using sampling functions with different sampling periods. The grating period of the whole wafer is uniform, which makes the fabrication by the conventional holography technology possible.

cycle change is small, because the derivative of the effective index modulation is zero when the duty cycle is 0.5, as shown in Fig. 8. For example, in Figs. 9 and 10, when the duty cycle is changed from 0.5 to 0.4, the threshold, the linewidth, and the SMSR are changed to be around 0.3 mA, 1 MHz, and 1 dB, respectively. Therefore, we can conclude that, in the fabrication of an ECT-based DFB laser, the proposed technique has a high tolerance to duty cycle errors.

B. Sampling Period

From (5), we can see that the lasing wavelength of the proposed equivalent CPM DFB laser can be approximated as

$$\lambda_L \approx 2n_{\text{eff}} \frac{P\Lambda}{P - \Lambda} \qquad (10)$$

which shows that the lasing wavelength is determined not only by the grating pitch, but also by the sampling period. Therefore, in the design of an equivalent CPM DFB laser, we can control the lasing wavelength by adjusting the sampling period of the SBG, while keeping the grating period unchanged, which makes the fabrication significantly simplified: based on the ECT, it is possible to fabricate DFB lasers with different lasing wavelengths on the same wafer with a homogeneous grating. The different lasing wavelengths are obtained by using sampling functions with different sampling periods, as can be seen from Fig. 11. In addition, the CPMs required in all of the DFB lasers could also be designed by modifying the sampling functions without complicating the grating structures. Therefore, in a DFB laser array, both the lasing wavelength and the chirp can be designed by controlling the sampling functions rather than the grating period.
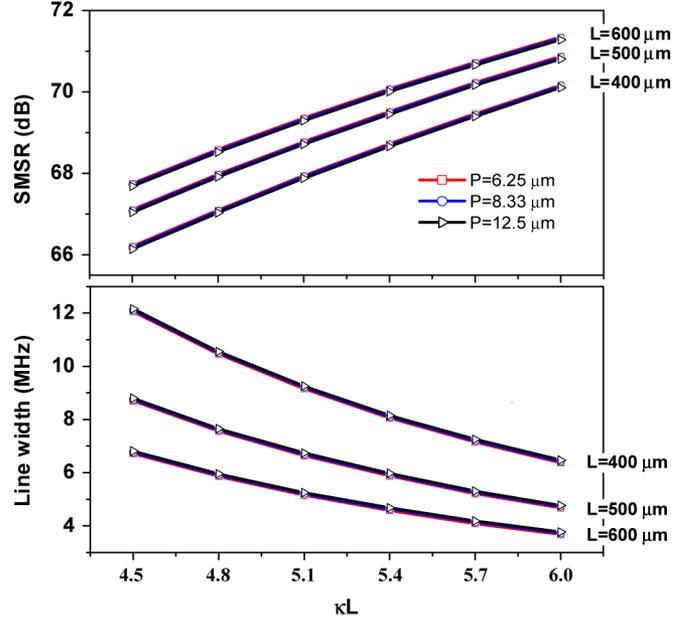
Fig. 12. Dependence of the SMSR and the linewidth on the laser length, grating strength, and the sampling period. The output power is kept at 6 mW in our simulation. Other parameters are the same as those listed in Table I.

If the DFB laser is used in a DWDM system, a wavelength resolution of at least 0.4 nm is required. Based on (10), we have

$$\Delta\lambda_L \approx -2n_{\text{eff}} \frac{\Lambda^2}{P^2} \times \Delta P. \qquad (11)$$

Therefore, a precision of 0.05 μm is then required in the sampling period, if the DFB laser is designed based on the parameters shown in Table I. However, for a conventional DFB laser, a wavelength resolution of 0.4 nm corresponds to a precision of 0.058 nm in the control of the grating period, which is about three orders of magnitude higher than the precision required in the proposed ECT. The use of the proposed ECT will greatly simplify the DFB laser and laser array fabrication.

In addition, from (6), we can see that the structure of the -1st-order subgrating, which is the effective grating for the DFB laser, will not change when the sampling period is changed. As a conclusion, the lasing performance will not be affected by the change of sampling period either. Fig. 12 shows the simulation results of the dependence of the linewidth and the SMSR on the change of the grating strength (κL) and the grating length. When the grating is lengthened or the κL is increased, the linewidth of the lasing spectrum will decrease and the SMSR will increase, the same as a conventional DFB laser does. However, the change of the sampling period shows no impact on the lasing performance, as shown in Fig. 12. This example confirms the theoretical analysis in Section II.

Based on the above analysis, we can see that, with the ECT, a DFB laser array can be achieved with all of the wavelengths having the same lasing performance. As an example, we design an DFB laser array that consists of three equivalent CPM DFB lasers with an identical grating length of 400 μm and grating period of 218.062 nm. The sampling periods are 7.69, 6.25, and 5.26 μm. As a result, the numbers of samples in the three DFB
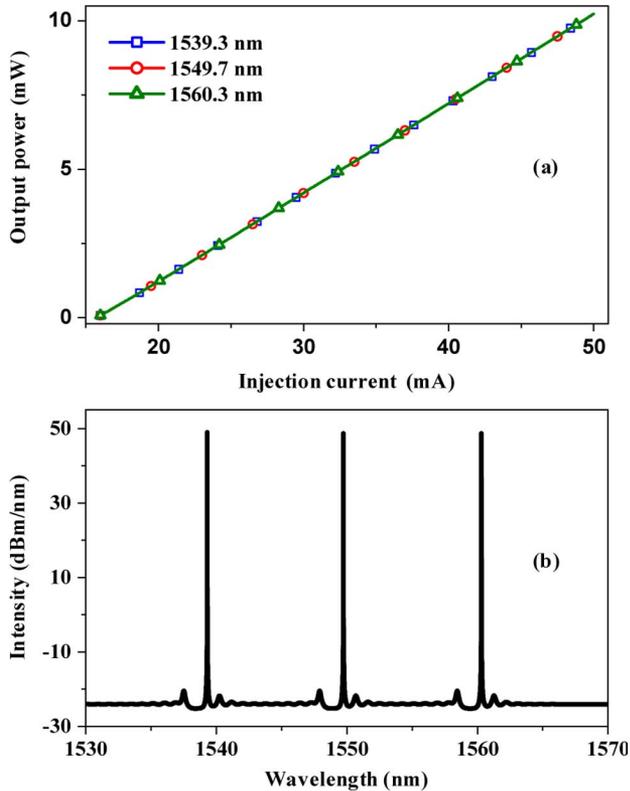
Fig. 13. (a) P–I curve of the CPM laser array. (b) Output spectrum of the CPM laser array.

lasers are 52, 64, and 76. Other parameters used in the design are the same as those used in the single-wavelength DFB laser discussed in Section II and listed in Table I. The laser array is then simulated with the results plotted in Fig. 13. Fig. 13(a) shows the P–I performance. It is seen that the three CPM DFB lasers have the same P–I performance. When the input current to the three lasers is 36 mA (corresponding to an output power of 6 mW for a single-wavelength equivalent CPM DFB laser), the laser array would start to lase with lasing wavelengths at 1539.3, 1549.7, and 1560.3 nm. The spectrum of the lasing output of the laser array is shown in Fig. 13(b). The same performance is achieved for the three lasing wavelengths. The results confirm that a laser array implemented based on the ECT would provide a high-performance operation. It should be emphasized here that the whole laser array has a homogeneous grating, which is different from a conventional DFB laser array, with different wavelengths having different grating periods. The key advantage of using the ECT to design an equivalent CPM DFB laser array is that the fabrication can be significantly simplified by using the conventional holography technology.

V. CONCLUSION

A proposal for the design of advanced semiconductor DFB lasers and DFB laser arrays with an equivalent chirp based on the ECT was presented. Theoretical analysis was performed, with the performance of the equivalent CPM DFB laser being evaluated, which was compared with a DFB laser with a true chirp. The characteristics such as the P–I performance, the light

distribution, the lasing spectrum, and the linewidth have been evaluated. The results showed that a DFB laser with an equivalent CPM would provide the same performance as a DFB laser with a true CPM. The performance of a DFB laser array designed based on ECT was also evaluated. The results confirmed that a DFB laser array implemented based on the ECT would provide a high-performance operation. The key advantage of the proposed technology is that a uniform grating is required in the whole wafer for both a single-wavelength DFB laser and a DFB laser array; therefore, the DFB laser or laser array can be fabricated using the conventional holography technology, which could significantly simplify the fabrication system and reduce the fabrication cost.

REFERENCES

[1] S. Akiba, M. Usami, and K. Utaka, "1.5- μm λ/4-shifted InGaAsP/InP DFB lasers," *J. Lightwave Technol.*, vol. 5, no. 11, pp. 1564–1573, Nov. 1987.

[2] P. Zhou and G. S. Lee, "Mode selection and spatial hole burning suppression of a chirped grating distributed feedback laser," *Appl. Phys. Lett.*, vol. 56, no. 15, pp. 1400–1402, Apr. 1990.

[3] P. Zhou and G. S. Lee, "Phase shifted distributed feedback laser with linearly chirped grating for narrow linewidth and high-power operation," *Appl. Phys. Lett.*, vol. 58, no. 4, pp. 331–333, Jan. 1991.

[4] M. Okai, T. Tsuchiya, K. Uomi, N. Chinone, and T. Harada, "Corrugation-pitch modulated MQW-DFB lasers with narrow spectral linewidth," *IEEE J. Quantum Electron.*, vol. 27, no. 6, pp. 1767–1772, Jun. 1991.

[5] M. Okai, M. Suzuki, and T. Taniwatari, "Strained multiquantum-well corrugation-pitch-modulated distributed feedback laser with ultranarrow (3.6 kHz) spectral linewidth," *Electron. Lett.*, vol. 29, no. 19, pp. 1696–1697, Sept. 1993.

[6] M. Mohrle, A. Sigmund, R. Steingruber, W. Furst, and A. Suna, "All-active tapered 1.55- μm InGaAsP BH-DFB laser with continuously chirped grating," *IEEE Photon. Technol. Lett.*, vol. 15, no. 3, pp. 365–367, Mar. 2003.

[7] D. J. Dougherty, R. E. Muller, P. D. Maker, and S. Forouhar, "Stitching-error reduction in gratings by shot-shifted electron-beam lithography," *J. Lightwave Technol.*, vol. 19, no. 10, pp. 1527–1531, Oct. 2001.

[8] J. Hong, W. P. Huang, T. Makino, and G. Pakulski, "Static and dynamic characteristics of MQW DFB lasers with varying ridge width," *IEE Proc. Optoelectron.*, vol. 141, no. 5, pp. 303–310, Oct. 1994.

[9] H. Hillmer, K. Magari, and Y. Suzuki, "Chirped gratings for DFB laser diodes using bent waveguides," *IEEE Photon. Technol. Lett.*, vol. 5, no. 1, pp. 10–12, Jan. 1993.

[10] J. Salzman, H. Olesen, A. M. Larsen, O. Albrektsen, J. Hanberg, J. Norregaard, B. Jonsson, and B. Tromborg, "Distributed feedback lasers with an S-bent waveguide for high-power single-mode operation," *IEEE J. Sel. Topics Quantum Electron.*, vol. 1, no. 2, pp. 346–355, Jun. 1995.

[11] D. F. Welch, F. A. Kish, S. Melle, R. Nagarajan, M. Kato, C. H. Joyner, J. L. Pleumeekers, R. P. Schneider, Jr., J. Bäck, A. G. Dentai, V. G. Dominic, P. W. Evans, M. Kauffman, D. J. H. Lambert, S. K. Hurtt, A. Mathur, M. L. Mitchell, M. Missey, S. Murthy, A. C. Nilsson, R. A. Salvatore, M. F. Van Leeuwen, J. Webjorn, M. Ziari, S. G. Grubb, D. Perkins, M. Reffle, and D. G. Mehuys, "Large-scale InP photonic integrated circuits: Enabling efficient scaling of optical transport networks," *IEEE J. Sel. Topics Quantum Electron.*, vol. 13, no. 1, pp. 22–31, Jan. 2007.

[12] S. H. Oh, J. U. Shin, Y. J. Park, S. B. Kim, S. Park, H. K. Sung, Y. S. Baek, and K. R. Oh, "Multiwavelength lasers for WDM-PON optical line terminal source by silica planar lightwave circuit hybrid integration," *IEEE Photon. Technol. Lett.*, vol. 19, no. 20, pp. 1622–1624, Oct. 2007.

[13] H. Hillmer and B. Klepser, "Low-cost edge-emitting DFB laser arrays for DWDM communication systems implemented by bent and tilted waveguides," *IEEE J. Quantum Electron.*, vol. 40, no. 10, pp. 1377–1383, Oct. 2004.

[14] Y. Dai, X. Chen, L. Xia, Y. Zhang, and S. Xie, "Sampled Bragg grating with desired response in one channel by use of a reconstruction algorithm and equivalent chirp," *Opt. Lett.*, vol. 29, no. 12, pp. 1333–1335, June 2004.

[15] D. Jiang, X. Chen, Y. Dai, H. Liu, and S. Xie, "A novel distributed feedback fiber laser based on equivalent phase shift," *IEEE Photon. Technol. Lett.*, vol. 16, no. 12, pp. 2598–2600, Dec. 2004.

[16] Y. Dai, X. Chen, J. Sun, Y. Yao, and S. Xie, "High-performance, high-chip-count optical code division multiple access encoders-decoders based on a reconstruction equivalent-chirp technique," *Opt. Lett.*, vol. 31, no. 11, pp. 1618–1620, June 2006.

[17] Y. Dai and X. Chen, "DFB semiconductor lasers based on reconstruction-equivalent-chirp technology," *Opt. Exp.*, vol. 15, no. 5, pp. 2348–2353, Mar. 2007.

[18] M. Okai, N. Chinone, H. Taira, and T. Harada, "Corrugation-pitch-modulated phase-shifted DFB laser," *IEEE Photon. Technol. Lett.*, vol. 1, no. 8, pp. 200–201, Aug. 1989.

[19] G. P. Agrawal and A. H. Bobeck, "Modeling of distributed feedback semiconductor lasers with axially varying parameters," *IEEE J. Quantum Electron.*, vol. 24, no. 12, pp. 2407–2414, Dec. 1988.

[20] J. E. A. Whiteaway, G. H. B. Thompson, A. J. Collar, and C. J. Armistead, "The design and assessment of λ/4 phase-shifted DFB laser structures," *IEEE J. Quantum Electron.*, vol. 25, no. 6, pp. 1261–1279, Jun. 1989.

[21] A. M. Sarangan, W.-P. Huang, and T. Makino, "Spectral domain modeling of distributed feedback lasers," in *Proc. SPIE*, Jun. 1997, vol. 2994, pp. 723–733.

[22] A. M. Sarangan, G. P. Li, W. P. Huang, and T. Makino, "Three-dimensional analysis of multi-wavelength DFB laser array," in *Proc. SPIE*, May 1996, vol. 2690, pp. 276–285.

Yitang Dai received the B.Sc. and Ph.D. degrees in electronic engineering from the Tsinghua University, Beijing, China, in 2002 and 2006, respectively.

Since June 2007, he has been a Postdoctoral Research Fellow with the Microwave Photonics Research Laboratory, School of Information Technology and Engineering, University of Ottawa, Ottawa, ON, Canada. His research interests include fiber Bragg gratings, optical CDMA, fiber lasers, microwave photonics, pulse shaping, semiconductor lasers, and optical sensors.

Jianping Yao (M'99–SM'01) received the Ph.D. degree in electrical engineering from the Université de Toulon, Toulon, France, in 1997.

He joined the School of Information Technology and Engineering, University of Ottawa, ON, Canada, in 2001, where he is currently a Professor, Director of the Microwave Photonics Research Laboratory, and Director of the Ottawa-Carleton Institute for Electrical and Computer Engineering. From 1999 to 2001, he held a faculty position with the School of Electrical and Electronic Engineering, Nanyang Technological University, Singapore. He spent three months as an Invited Professor with the Institut National Polytechnique de Grenoble, France, in 2005. His research has focused on microwave photonics, which includes all-optical microwave signal processing, photonic generation of microwave, millimeter-wave and THz, radio-over-fiber, UWB-over-fiber, fiber Bragg gratings for microwave photonics applications, and optically controlled phased array antenna. His research interests also include fiber lasers, fiber-optic sensors, and bio-photonics. He is an Associate Editor of the *International Journal of Microwave and Optical Technology*. He has authored or coauthored over 200 papers in refereed journals and conference proceeding.

Dr. Yao is a member of SPIE and the Optical Society of America and a senior member of the IEEE Lasers and Electro-Optics Society and the IEEE Microwave Theory and Techniques Society. He is a Registered Professional Engineer of Ontario and is on the Editorial Board of the IEEE TRANSACTIONS ON MICROWAVE THEORY AND TECHNIQUES. He was the recipient of the 2005 International Creative Research Award of the University of Ottawa and the 2007 George S. Glinski Award for Excellence in Research. He was named the University Research Chair in Microwave Photonics in 2007.